Evolution of the pseudogap in $Sr_{1-x}Y_xAl_2Si_2$ ($x = 0$, 0.05, 0.1, and 0.15) probed via ^{27}Al nuclear magnetic resonance

C. P. Fang,[1] C. S. Lue,[1,*] and Ben-Li Young[2]

[1]*Department of Physics, National Cheng Kung University, Tainan 70101, Taiwan*

[2]*Department of Electrophysics, National Chiao Tung University, Hsinchu 30010, Taiwan*

(Received 8 April 2010; revised manuscript received 9 February 2011; published 28 March 2011)

With the aim of providing microscopic information about the electronic characteristics of $SrAl_2Si_2$ and effects of chemical substitution on its pseudogap features, we carried out a study on $Sr_{1-x}Y_xAl_2Si_2$ ($x = 0$, 0.05, 0.1, and 0.15) by means of ^{27}Al nuclear magnetic resonance (NMR) spectroscopy. For stoichiometric $SrAl_2Si_2$, the temperature-dependent NMR Knight shift and spin-lattice relaxation rate are associated with a sharp feature in the electronic density of state within a pseudogap at around the Fermi level. On the other hand, the NMR observations for Y-substituted compounds exhibit ordinary metallic behavior, suggesting that the Fermi level has moved out of the pseudogap for these materials, resulting in the dominant Korringa process responsible for the observed relaxation rates.

DOI: 10.1103/PhysRevB.83.113105 PACS number(s): 71.20.−b, 76.60.−k

After the discovery of superconductivity in MgB_2 there has been great interest in related compounds with hexagonal graphitelike AlB_2-type structure.[1–3] The layered ternary alumino silicides Sr-Al-Si have thus attracted considerable attention because one of the systems SrAlSi, isostructural to MgB_2, is also a superconductor with T_C of 4.2–5.1 K.[4,5] In addition to SrAlSi, there is another ternary layered Sr-Al-Si system, $SrAl_2Si_2$, which crystallizes in the trigonal La_2O_3-type structure (space group $\bar{3}m1$).[6] Within this structure, Si and Al atoms are arranged in chemically ordered double-corrugated hexagonal layers, with Sr atoms alternating between them. $SrAl_2Si_2$ has been speculated to be a semimetal based on the negative temperature coefficient with a broad maximum near 160 K in the electrical resistivity (ρ), and no evidence of superconducting behavior has been found above 2 K.[6] The observed semimetallic response is typically due to the thermal activation of carriers across a pseudogap, estimated to be about 40 meV.[6] In addition, the Seebeck coefficient (S) exhibits a broad minimum at around 120 K with a magnitude of about 100 $\mu V/K$.[7] Upon increasing temperature, the absolute value of S decreases but the sign remains negative up to 1200 K, indicating that the n-type carriers dominate the transport while the minority p-type carriers are thermally excited to reduce the magnitude of S.[6]

A pseudogap appearing at the electronic density of states (DOS) around the Fermi level (E_F) is a common occurrence in transition-metal–metalloid compounds.[8] $CaAl_2Si_2$, isostructural to $SrAl_2Si_2$, and some silicides such as $SrSi_2$, also feature Fermi-level pseudogaps which were found to govern the electronic properties of the materials.[9–14] In general, the pseudogap characteristics are very sensitive to external effects such as chemical substitution. Hence, altering the composition allows a change of the electronic properties, and thus provides valuable information about the influence of the local environment on the structural and electronic behavior of gapped materials. With this motivation, we investigate the effects of yttrium substitution on the electronic nature of $SrAl_2Si_2$ by means of nuclear magnetic resonance (NMR) spectroscopy. The replacement of Sr by Y would cause a band structure modification since Y has one more electron in its valence shell than Sr, providing an opportunity for understanding how the semimetallic character behaves under doping with Y.

Part of our initial interest in $SrAl_2Si_2$ was in looking for superconductivity by substituting elements with a small atomic radius which would effectively produce a positive chemical pressure as Y has a smaller atomic size than Sr. Indeed, we have seen diamagnetic responses in several specimens below 4.3 K under a low-field magnetization measurement, pointing to the presence of superconducting behavior at low temperatures. However, we further identified this phenomenon to be the superconductivity of SrAlSi based on the identical T_C value and extremely low magnetic shielding fraction of these materials.

Samples studied here were prepared from 99% Sr, 99.9% Y, 99.9% Al, and 99.999% Si by mixing appropriate amounts of elemental metals. They were placed in a water-cooled copper crucible and then were melted several times in an Ar arc-melting furnace. The resulting ingots were annealed in a vacuum-sealed quartz tube at 800 °C for two days, followed by furnace cooling. A Cu $K\alpha$ x-ray analysis on powdered samples is consistent with the expected La_2O_3-type structure. We performed a more detailed analysis of the x-ray data, in which the La_2O_3-type structure was refined with the Rietveld method. We thus obtained the lattice constants, a and c, for each individual composition. The variation of lattice constant as a function of x is illustrated in Fig. 1. It clearly demonstrates that the constants gradually decrease with x, indicating that the Sr sites are successfully replaced by Y atoms, according to Vegard's law.

NMR experiments were performed under a constant field of 6.9437 T. Measurements extending up to 515 K for $SrAl_2Si_2$ allow us to examine the feature of the pseudogap. ^{27}Al NMR powder patterns were mapped out by integrating spin echo signals. Within the $P\bar{3}m1$ phase, the axially symmetric Al site results in a one-site NMR spectrum for each of the studied material. The observed room-temperature powder patterns for all $Sr_{1-x}Y_xAl_2Si_2$ alloys are shown in Fig. 2. The central transition line width essentially arises from the simultaneous presence of the anisotropic Knight shift and the second-order quadrupole interactions.[15] Both effects have a weak temperature dependence, and we indeed found

 ©2011 American Physical Society

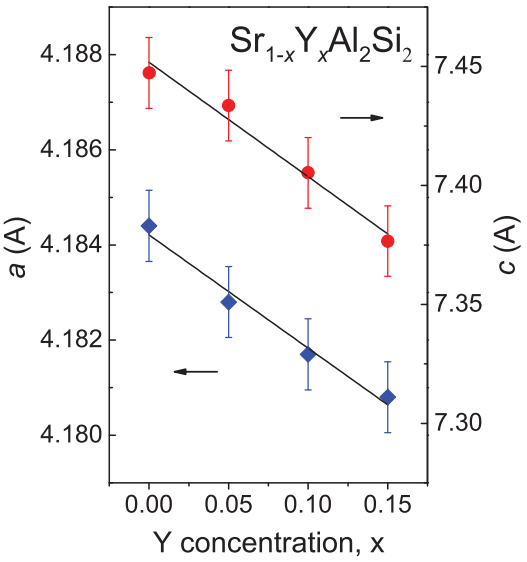

FIG. 1. (Color online) Variation of lattice constant versus Y concentration x in $Sr_{1-x}Y_xAl_2Si_2$.

little change in the linewidth within the measured temperature range. Note that a minor ^{27}Al NMR central transition line from SrAlSi appears in all Y-substituted samples, as marked by an arrow in each spectrum. This result confirms the existence of a minority phase of SrAlSi which could be responsible for the observed superconducting behavior below 4.3 K. It also suggests that a complete isolation from this impurity phase may not be possible using our growth method for preparing the $Sr_{1-x}Y_xAl_2Si_2$ alloys.

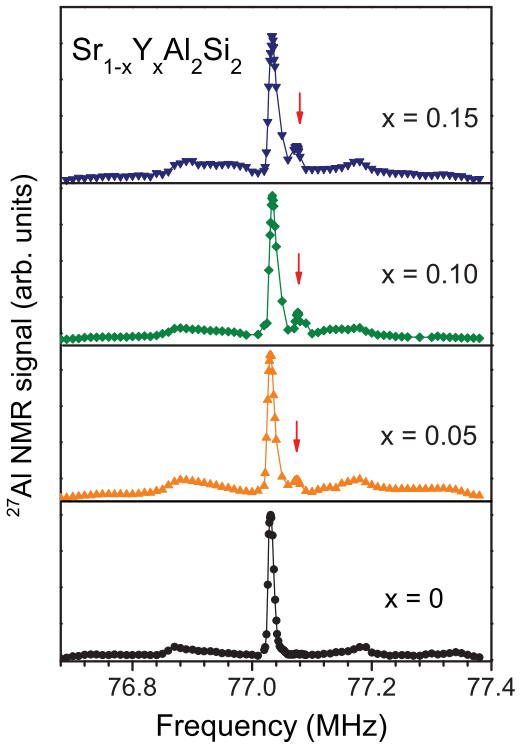

FIG. 2. (Color online) Fully resolved ^{27}Al NMR powder patterns for $Sr_{1-x}Y_xAl_2Si_2$. Each arrow indicates the ^{27}Al NMR central transition of SrAlSi.

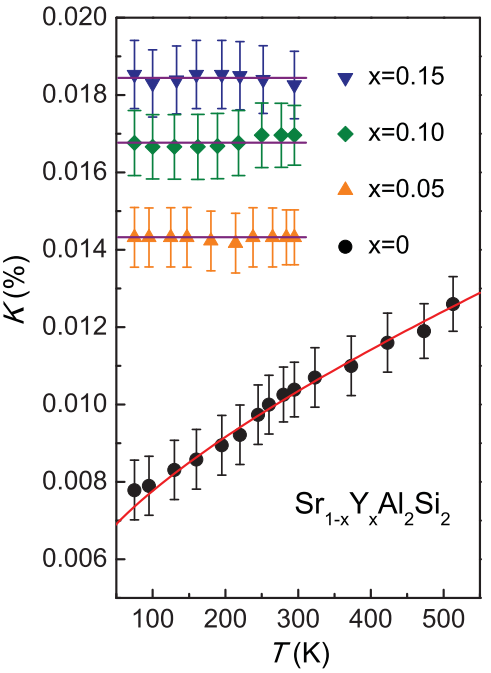

FIG. 3. (Color online) Temperature variation of the observed ^{27}Al Knight shifts for $Sr_{1-x}Y_xAl_2Si_2$. The solid curve is a fit to $K(T) = K_0 + A_1T^{\varepsilon}$ based on the model electronic DOS of $SrAl_2Si_2$. Horizontal lines: indications of the temperature-independent Knight shifts for $x > 0$.

In principle, each pattern consists of a central transition peak ($m = \frac{1}{2} \leftrightarrow -\frac{1}{2}$) with four satellite lines corresponding to the quadrupole parameter. Since the first-order quadrupole shift is the main effect shaping the satellite line, the effect of disorder should strongly broaden the satellite line shapes of $Sr_{1-x}Y_xAl_2Si_2$. As a matter of fact, the edge feature of the quadrupole wings gradually smears out as Y content increases. For the present $Sr_{1-x}Y_xAl_2Si_2$, the quadrupole frequency ν_Q was determined directly from these lines. The obtained $\nu_Q = 0.31 \pm 0.01$ MHz remains nearly unchanged with different doping levels x and this value is slightly smaller than that of $CaAl_2Si_2$ ($\nu_Q = 0.36 \pm 0.02$ MHz),[11] indicating weaker quadrupole interactions in $Sr_{1-x}Y_xAl_2Si_2$.

In Fig. 3, we display the temperature dependence of the observed ^{27}Al Knight shifts (K) for $Sr_{1-x}Y_xAl_2Si_2$. Here the value of K was determined from the center of gravity of each spectrum with respect to an aqueous $AlCl_3$ solution reference. The error bar was related to the accuracy of the determination of the center of gravity. Except for the stoichiometric $SrAl_2Si_2$, the Knight shifts show nearly T-independent behavior at all temperatures, a typical characteristic for nonmagnetic metals. Thus, the T-independent Knight shift (K_0) is mainly associated with the Fermi-contact Knight shift (K_s) which is connected to the number of s-character carriers in the ground state.[16] As indicated in Table I, the magnitude of K_0 becomes larger with increasing x in $Sr_{1-x}Y_xAl_2Si_2$, indicative of an increase in the s-character Fermi-level DOS, $g_s(E_F)$.

On the other hand, the Knight shift of $SrAl_2Si_2$ exhibits a shift to higher frequencies with increasing temperature in addition to a low-T constant term. Since the Knight shift probes the electronic DOS within a few k_BT around E_F, the thermally

TABLE I. Temperature-independent Knight shift in ppm, Korringa constant in 10^{-3} s^{-1} K^{-1}, Korringa ratio, and the Fermi-level s DOS in units of 10^{-3} states/eV atom deduced from K_0 and $1/T_{1K}T$.

x	K_0	$1/T_{1K}T$	R	$g_s^K(E_F)$	$g_s^R(E_F)$
0	55	0.34	2.3	4.9	3.7
0.05	142	4.7	1.11	12.9	12.3
0.10	168	7.1	1.03	15.2	15.1
0.15	184	8.2	1.07	16.6	16.2

activated behavior for $K(T)$ implies a sharp DOS feature in $SrAl_2Si_2$ near E_F. Indeed, the observation of the negative sign with a minimum in the Seebeck coefficient of $SrAl_2Si_2$ suggests that the corresponding E_F should locate at the rapid rising portion of the DOS.[6,7] Therefore, it is realistic to approximate the electronic DOS by $g(E) = g_0 + A \mid E_F - E \mid^{\varepsilon}$, where g_0 is the residual DOS at E_F and the power ε reflects the shape of the conduction band.[17] Under this approximation, the observed Knight shift follows $K(T) = K_0 + A_1 T^{\varepsilon}$. We found that the fitting is quite satisfactory with the data of $SrAl_2Si_2$, shown as a solid curve in Fig. 3. The fit reveals the values of $K_0 = 5.5 \times 10^{-5}$ and $A_1 = 9 \times 10^{-7}$ $K^{-0.7}$ with $\varepsilon = 0.7 \pm 0.1$.

The temperature dependence of the spin-lattice relaxation rate $(1/T_1)$ was measured using the inversion recovery method. We recorded the signal strength by integrating the recovered spin echo signal. In this experiment, the relaxation process involves adjacent pairs of spin levels, and the nuclear magnetization $M(t)$ recovery for the central transition with $I = 5/2$ follows

$$\frac{M(t)}{M(\infty)} = 1 - 2\alpha(0.0286e^{-t/T_1} + 0.178e^{-6t/T_1} + 0.793e^{-15t/T_1}). \quad (1)$$

Here α is a fractional value derived from the initial conditions used in our experiments. Our T_1 values were thus obtained by fitting to this multiexponential recovery curve, and several fitting results for different compositions measured at different temperatures are presented in Fig. 4. We show a plot of $1/T_1$ versus temperature for the studied $Sr_{1-x}Y_xAl_2Si_2$ alloys in Fig. 5. Except for $SrAl_2Si_2$, the $1/T_1$'s exhibit Korringa relaxation behavior (constant T_1T), which is consistent with the Knight shift observation. For $SrAl_2Si_2$, $1/T_1$appears to rise rapidly with increasing temperature, and the observed temperature variation should obey the form (by analogy to the Knight shift) as[17]

$$\frac{1}{T_1} = CT + A_2T^{1+\varepsilon} + A_3T^{1+2\varepsilon}. \quad (2)$$

Here the parameter $C \equiv 1/T_{1K}T$ represents a constant term of $1/T_1$ with the subscript K denoting the Korringa process. Using the same parameter $\varepsilon = 0.7$ obtained from the Knight shift analysis, we could reproduce the temperature dependence of $1/T_1$ according to Eq. (2), drawn as a solid curve in Fig. 5. We thus extracted $C = 3.4 \times 10^{-4}$ s^{-1} K^{-1}, $A_2 = 2 \times 10^{-5}$ $s^{-1}K^{-1.7}$, and $A_3 = 2.6 \times 10^{-7}$ s^{-1} $K^{-2.4}$ from this fit for $SrAl_2Si_2$. It is noticeable that these fitting parameters yield a dimensionless $K_0A_2/CA_1 = 3.6$, which is greater than the value of 2 as K_0 is entirely associated with s electrons. This discrepancy indicates that additional contributions such as the orbital shift (K_{orb}) to K_0 should not be neglected in $SrAl_2Si_2$.

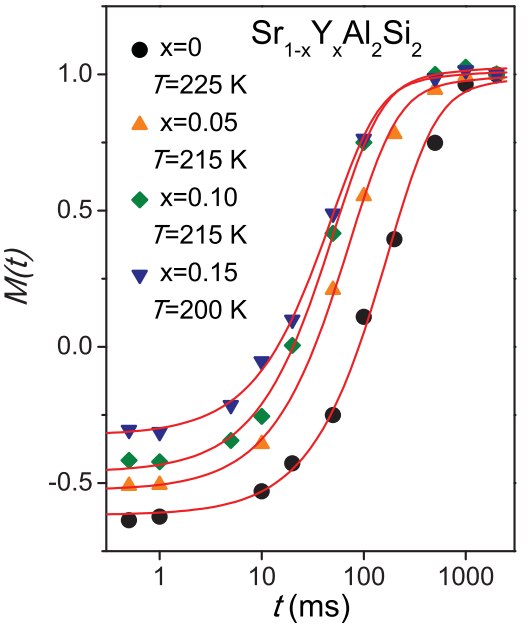

FIG. 4. (Color online) Representative nuclear magnetization recovery curves normalized by $M(\infty)$ of different compositions at various temperatures for $Sr_{1-x}Y_xAl_2Si_2$.

Note that $1/T_1$ for all Y-substituted compounds exhibits no such thermally activated response. This can be attributed to the fact that each additional Y should contribute more electrons in the mixed alloys. As a consequence, E_F shifts toward a higher DOS where the variation of the DOS for energies within

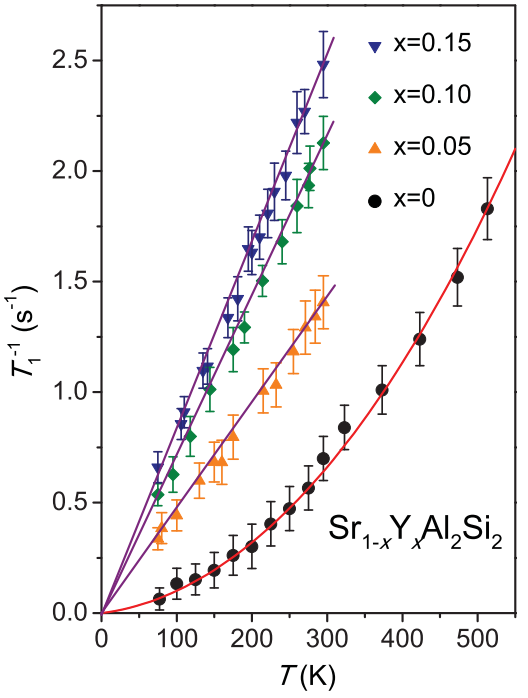

FIG. 5. (Color online) Temperature variation of the ^{27}Al spin-lattice relaxation rates for $Sr_{1-x}Y_xAl_2Si_2$. The solid curve is the fitted function according to Eq. (2) for $SrAl_2Si_2$. Each straight line represents a linear fit to the Korringa behavior for $x > 0$.

$k_B T$ is not important, resulting in the dominant Korringa behavior in $1/T_1$ as observed. A convincing demonstration for the Korringa process can be established from the Korringa ratio $R \equiv K_0^2 T_{1K} T/S$ where $S = 3.868 \times 10^{-6}$ s K for ^{27}Al is derived from the contact interaction with s electrons for the Knight shifts and relaxation rates. As one can see from Table I, the obtained ratios close to unity (except for $SrAl_2Si_2$) confirm that the contact electrons are responsible for both K_0 and T_{1K}. For $SrAl_2Si_2$, however, the relatively high ratio $R = 2.3$ is very likely due to an additional contribution from $K_{\rm orb}$ which becomes important as the observed shift is extremely small.

According to the noninteracting electron picture, the s-contact Knight shift can be expressed by $K_s = 2\mu_B H_{hf}^s g_s^K(E_F)$. Here μ_B is the Bohr magneton, H_{hf}^s is the hyperfine field of the s electrons, and $g_s^K(E_F)$ is the s DOS at the Fermi level in units of states/eV spin deduced from Knight shifts. With the estimate of $H_{hf}^s \sim 1.9 \times 10^6$ G calculated for Al metals,[15] we obtained each $g_s^K(E_F)$ value with the results listed in Table I. It is apparent that the magnitude of $g_s^K(E_F)$ gradually increases with increasing x in $Sr_{1-x}Y_xAl_2Si_2$, in agreement with the fact that each additional Y should contribute more electrons in the mixed alloys.

The Korringa contribution of $1/T_{1K}T$ can be evaluated to provide a measure of the Al s Fermi-level DOS, $g_s^R(E_F)$, as reported previously for other aluminides.[18–20] In the absence of collective electron effects, the relaxation rate is simply governed by the initial occupied and final unoccupied electronic states, associated with the hyperfine field arising from contact electrons. Therefore, $1/T_{1K}T$ can be written as

$$\frac{1}{T_{1K}T} = 2hk_B\left[\gamma_n H_{hf}^s g_s^R(E_F)\right]^2, \tag{3}$$

where h is the Planck constant, k_B is the Boltzmann constant, and γ_n is the Al nuclear gyromagnetic ratio. From the determined $1/T_{1K}T$ values, we can obtain $g_s^R(E_F) = 0.0037$ states/eV atom for $SrAl_2Si_2$, and fewer than 0.0068 states/eV atom measured in this way for $CaAl_2Si_2$.[11] We also extracted $g_s^R(E_F)$ values for other compositions, showing a gradual increase with increasing x in $Sr_{1-x}Y_xAl_2Si_2$, which is consistent with the Knight shift analysis.

The NMR observations provide microscopic evidence for the pseudogap feature in $SrAl_2Si_2$ while the pseudogap signature is not evident on replacing Sr by Y, when the compound shows typical metallic characteristics instead. It is worth mentioning that quasicrystalline materials which also feature Fermi-level pseudogaps with sharp DOS structures exhibit similar NMR responses in the Knight shift as well as the relaxation rate.[17,21] Analyses based on the same form of the DOS yielded consistent results and gave a good understanding of the electronic properties of the materials. With this comparison, the electronic characteristics of $SrAl_2Si_2$ are very similar to those cases. This also indicates that the electronic structure of $Sr_{1-x}Y_xAl_2Si_2$ obtained from the present NMR results is basically reliable.

In summary, our NMR observations have provided a local picture of the electronic evolution of $Sr_{1-x}Y_xAl_2Si_2$, revealing that $SrAl_2Si_2$ possesses a pseudogap with rapidly changing DOS with energy in the vicinity of E_F. The variation of the band edge is approximately proportional to $|E_F - E|^{0.7}$, obtained from the Knight shift and the relaxation rate analyses. Upon substituting Y onto the Sr sites, the sharp band feature smears out due to the increase in the electronic carriers in the mixed alloys, leading to typically metallic behavior in the NMR measurements for $Sr_{1-x}Y_xAl_2Si_2$.

We are grateful for the support from the National Science Council of Taiwan under Grant No. NSC-98-2112-M-006-011-MY3 (C.S.L.).

*cslue@mail.ncku.edu.tw

[1] M. Imai, E. Abe, J. Ye, K. Nishida, T. Kimura, K. Honma, H. Abe, and H. Kitazawa, Phys. Rev. Lett. **87**, 077003 (2001).
[2] H. T. Su, C. S. Lue, and Y. K. Kuo, J. Appl. Phys. **104**, 093105 (2008).
[3] C. P. Fang, C. S. Lue, Y. D. Hsu, and Y. K. Kuo, J. Appl. Phys. **108**, 073911 (2010).
[4] M. Imai, K. Nishida, T. Kimura, H. Kitazawa, H. Abe, H. Kito, and K. Yoshii, Physica C **382**, 361 (2002).
[5] B. Lorenz, J. Lenzi, J. Cmaidalka, R. L. Meng, Y. Y. Sun, Y. Y. Xue, and C. W. Chu, Physica C **383**, 191 (2002).
[6] S. M. Kauzlarich, C. L. Condron, J. K. Wassei, T. Ikeda, and G. J. Snyder, J. Solid State Chem. **182**, 240 (2009).
[7] Y. K. Kuo (private communication).
[8] M. Weinert and R. E. Watson, Phys. Rev. B **58**, 9732 (1998).
[9] M. Imai, H. Abe, and K. Yamada, Inorg. Chem. **43**, 5186 (2004).
[10] G. Q. Huang, M. Liu, L. F. Chen, and D. Y. Xing, J. Phys.: Condens. Matter **17**, 7151 (2005).
[11] C. S. Lue, S. Y. Wang, and C. P. Fang, Phys. Rev. B **75**, 235111 (2007).
[12] Y. K. Kuo, K. M. Sivakumar, J. I. Tasi, C. S. Lue, J. W. Huang, S. Y. Wang, D. Varshney, N. Kaurav, and R. K. Singh, J. Phys.: Condens. Matter **19**, 176206 (2007).
[13] M. Imai, T. Naka, T. Furubayashi, H. Abe, T. Nakama, and K. Yagasaki, Appl. Phys. Lett. **86**, 032102 (2005).
[14] C. S. Lue, M. D. Chou, N. Kaurav, Y. T. Chung, and Y. K. Kuo, Appl. Phys. Lett. **94**, 192105 (2009).
[15] *Metallic Shifts in NMR*, edited by G. C. Carter, L. H. Bennett, and D. J. Kahan (Pergamon, Oxford, 1977).
[16] C. P. Slichter, *Principles of Magnetic Resonance* (Springer-Verlag, New York, 1990).
[17] X.-P. Tang, E. A. Hill, S. K. Wonnell, S. J. Poon, and Y. Wu, Phys. Rev. Lett. **79**, 1070 (1997).
[18] C. S. Lue, B. X. Xie, S. N. Horng, J. H. Su, and J. Y. Lin, Phys. Rev. B **71**, 195104 (2005).
[19] C. S. Lue, J. Y. Lin, and B. X. Xie, Phys. Rev. B **73**, 035125 (2006).
[20] C. S. Lue, B. X. Xie, and C. P. Fang, Phys. Rev. B **74**, 014505 (2006).
[21] J. Dolinsek, M. Klanjsek, T. Apih, A. Smontara, J. C. Lasjaunias, J. M. Dubois, and S. J. Poon, Phys. Rev. B **62**, 8862 (2000).